

# A 3D intensity imaging for stainless histopathology

Jie Li<sup>1,\*</sup>, Weiwei Goh<sup>1</sup>, N.Z. Jhanjhi<sup>1</sup> and Bowen Li<sup>2</sup>

<sup>1</sup>Digital Health and Medical Advancement Impact Lab, School of Computer Science, Taylor's University, Subang Jaya, Malaysia

<sup>2</sup>Dermatology Department, Ningxia Yiyang Hospital, Ningxia, China

**Abstract.** Histopathological image analysis is a cornerstone of cancer diagnosis, but its effectiveness is often limited by variability in staining protocols and imaging conditions across laboratories. This paper presents a novel 3D intensity-based stainless imaging framework integrates stain normalization and deep learning to standardize tissue visualization and improve diagnostic accuracy. Our method transforms conventional 2D histopathology images into 3D intensity maps, leveraging the Beer-Lambert law for stain normalization to mitigate staining variability while preserving critical tissue architecture. We validate our approach on the 305 randomly selected samples from LC-25000 (benign and malicious colon histopathology images) using Structural Similarity Index (SSIM) to quantify preservation of diagnostically relevant structures. Results demonstrate high SSIM scores for normalized 2D images ( $0.92 \pm 0.03$ ) and 3D reconstructions ( $0.88 \pm 0.05$ ), confirming structural fidelity during dimensionality expansion. The 3D intensity maps serve as input to a 3D convolutional neural network (CNN), enabling robust feature learning and achieving superior accuracy compared to traditional 2D methods.

## 1 Introduction

In cancer diagnosis, the intensity map is a fundamental and crucial concept in medical image processing and analysis [1]. It is not a specific detection method, but rather the core data that constitutes almost all medical images (such as histopathology, CT, MRI, PET, and ultrasound) for different modalities in the detection, diagnosis, staging, treatment, and efficacy evaluation of cancer [2]. The value of pixel (2D) or voxel (3D) in the intensity map represents the physical properties of the tissue at that location under a specific imaging mode.

In the field of cancer diagnosis using histopathology images, the variability in staining protocols and the presence of irrelevant color information can introduce significant noise [3], and it potentially hinders the performance of convolutional neural networks (CNNs) [2, 3]. Intensity maps offer a promising solution by suppressing these irrelevant color variations and highlighting diagnostically significant structures, such as nuclei density and glandular architecture [4]. Thereby, the Intensity map empowers the CNN to focus on features most relevant to cancer identification. Furthermore, intensity maps can facilitate stain

---

\* Corresponding author: [lijiesat@hotmail.com](mailto:lijiesat@hotmail.com)

normalization, and reduce the impact of inter-laboratory differences and ensure more consistent input data for automated analysis [5].

However, the use of intensity maps faces challenges. Full-color histopathology images to intensity maps may result in the loss of valuable color and texture information, which can be critical for distinguishing between certain cell types and subtle pathological features [3]. Additionally, over-simplification through intensity mapping may obscure complex patterns that are best appreciated in the original color space [6]. Therefore, while an intensity map-based CNN system has the potential to enhance robustness and accuracy in colon cancer detection, careful consideration must be given to balancing the benefits of noise reduction and feature enhancement against the risk of information loss and over-simplification.

The objective of this paper is to propose a 3D intensity based stainless imaging method for histopathological cancer diagnosis to reduce stain while remains features of original images. The motivation of the research is to improve the usefulness of the AI medical solution in real clinical settings. The significance of the paper is the innovative proposed approach for a fast and reliable tool in quantitative diagnosis.

## 2 Related Works

From 2D to 3D visualization, intensity is dimensionized as the z-axis for abstract imaging. By mapping 2D intensity values into a 3D surface, researchers extract features such as surface roughness, peak distribution, and texture, which are then used for classification or segmentation [2]. Some studies [2, 7, 8] use intensity maps as additional channels for CNNs, allowing the network to learn from both spatial and intensity-based cues. Takahashi, et al. [9] developed a CNN model using multiple degrees of maximum-intensity projection for PET/CT image classification in breast cancer. Naglah, et al. [10] studied the heterogeneity in intensity variance between T2-weighted images of MRI for the thyroid cancer diagnosis.

3D plots help pathologists and AI systems visualize complex tissue architecture, making it easier to spot abnormalities [11]. First of all, with integration with CNN architecture, 3D intensity maps could facilitate 3D convolutional networks for richer feature learning [12]. Second, the use of 3D intensity model encourages the multi-modal fusion in medical signal processing [13]. Combining 3D intensity features with other modalities (e.g., immunohistochemistry, genomics) for comprehensive cancer profiling [14]. Lastly, the use of 3D intensity imaging could automate grading. Rao, et al. [15] designed a prediction and classification model of Alzheimer's disease using 3D MR images.

The transformation of 2D histopathology images into 3D intensity maps is a promising direction in computational pathology [16, 17]. It enables the extraction of advanced features and supports the development of more accurate and robust cancer diagnostic systems [17]. As deep learning and image analysis techniques evolve, the use of 3D intensity information is expected to become increasingly central in digital pathology workflows [18].

## 3 Methods

### 3.1 Data and Sampling

In this research, experiment samples were collected from the LC-250000 dataset [19], which contains 10,000 colon and 15,000 lung histopathology tissue images. In this research, there were 305 randomly selected benign and malicious images used as experiment dataset.

### 3.2 Algorithm Design and Development

The intensity transformation from 2D histopathological image involves the intensity calculation. Let  $I(x, y)$  represent the original 2D histopathology image where  $(x, y)$  are the spatial coordinates, and Eq.1 represents the RGB color values at each pixel location.

$$I(x, y) = \begin{bmatrix} R_{(x,y)} \\ G_{(x,y)} \\ B_{(x,y)} \end{bmatrix} \quad (1)$$

The transformation to a 3D intensity map  $M(x, y, z)$  can be expressed as in Eq.2

$$M(x, y, z) = f(I(x, y), z) \quad (2)$$

However, regarding the occurrence of stain, the normalization shows optical density ( $O$ ) of the  $I(x, y)$  using Beer-Lambert law [20] in Eq.3 where  $I_0$  is the background color of the image:

$$O(x, y) = -\log\left(\frac{I(x,y)+1}{I_0+1}\right) \quad (3)$$

The color deconvolution takes place and stain are normalized as  $I_{Norm}(x, y)$  shown in the Eq.4 where standard deviation ( $\sigma$ ) and mean ( $\mu$ ) for original and stainless sample sets.

$$I_{Norm}(x, y) = \frac{\sigma_{target}}{\sigma_{original}}(O(x, y) - \mu_{original}) + \mu_{target} \quad (4)$$

Hence, the stain-normalized image could be reconstruct as shown in Eq.5

$$I_{Norm}(x, y) = I_0 * e^{(O(x,y))} \quad (5)$$

Specifically, the grayscaling transformation for  $I_{norm}(x, y)$  can be written as the intensity value  $I_{grayscale}(x, y)$  in Eq.6.

$$I_{grayscale}(x, y) = \overrightarrow{I_{norm}} ** Sensitivity_{(R,G,B)} \quad (6)$$

$$I_{grayscale}(x, y) = \begin{bmatrix} R_{(x,y)} \\ G_{(x,y)} \\ B_{(x,y)} \end{bmatrix} \begin{bmatrix} .299 \\ .587 \\ .114 \end{bmatrix} \quad (7)$$

The coefficients of Sensitivity for RGB channels are (0.299), (0.587), and (0.114), and these parameters are derived from the perceived luminance of the colors by the human eye. Different colors contribute differently to the perception of brightness [21]. For a grayscale intensity transformation, Eq.2 can be defined and categorized based on  $I_{grayscale}(x, y) = z$  in Eq.8.

$$M(x, y, z) = \begin{cases} 0 & I_{grayscale}(x, y) \neq z \\ 1 & I_{grayscale}(x, y) = z \end{cases} \quad (8)$$

In a whole slide image, for the intensity value on the z-axis can be written in Eq.9.

$$M(x, y, z) = (x, y, I_{grayscale}(x, y)) \quad (9)$$

This sequence ensures that the intensity map for visualization is not biased by staining differences and makes downstream analysis more robust and reproducible.

### 3.3 Measures

The Structural Similarity Index (SSIM) compares luminance, contrast, and structure of images before ( $A$ ) and after ( $B$ ) the application of image processing in Eq.10.

$$SSIM(A, B) = \frac{(2\mu_A\mu_B + C_1)(2\sigma_{AB} + C_2)}{(\mu_A^2 + \mu_B^2 + C_1)(\sigma_A^2 + \sigma_B^2 + C_2)} \quad (10)$$

SSIM is widely used to evaluate stain normalization quality where higher SSIM ( $\geq 0.9$ ) confirms preserved tissue structure post-normalization in histopathology image processing.

## 4 Result and Discussion

**Table 1.** SSIM Examination Result (n = 305).

Comparison	Mean SSIM ( $\pm$ SD)	Interpretation
Original vs. Normalized (2D)	0.92 $\pm$ 0.03	Stain variability removed, structure intact.
Original vs. 3D Reconstructed	0.88 $\pm$ 0.05	Minor loss from 2D $\rightarrow$ 3D conversion.

In machine learning applications, color and intensity are critical features for tissue classification and cancer diagnosis. standardize the color appearance of histopathology images ( $I(x, y)$ ), effectively reducing the impact of staining variability. In this process, the image is first converted from the RGB color space to optical density ( $O$ ) space, which linearizes the relationship between stain concentration and observed color. The  $O(x, y)$  values are then adjusted to match the statistical properties (mean and standard deviation) of a reference or target stain profile. Table 1. indicated the SSIM variance from original to normalized and then to 3D reconstructed. This experiment began with a histopathology image (Fig. 1) representing a tissue section stained for microscopic examination. The original image exhibits the natural variability inherent in histological staining processes. This variability can arise from differences in staining protocols, reagent concentrations, and scanner settings, so as to inconsistencies in color and intensity across different slides, even when they represent similar tissue types. Experimental result in Table 1. pointed the SSIM varies from 0.89 to 0.95, meaning stain variability removed.

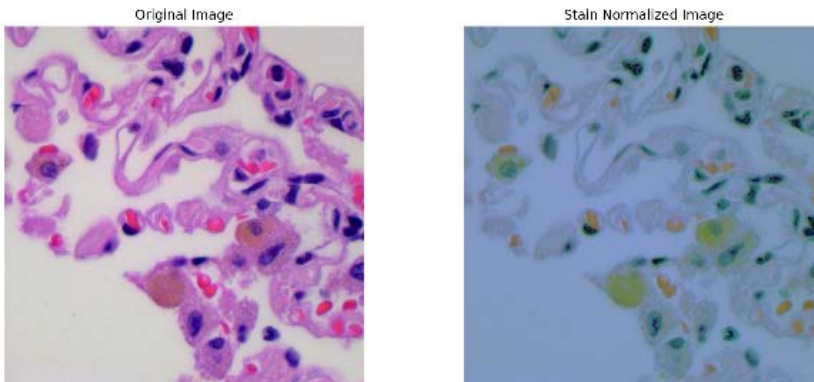


**Fig. 1.** Original and Stainless Histopathology Image.

As shown in the Fig.2, the  $X$  and  $Y$  axes represent the spatial coordinates (pixels) of the image, while the  $Z$  axis shows the normalized grayscale intensity ( $I_{grayscale}(x, y)$ ) at each point. The color gradient on the surface highlights regions of varying intensity, which can correspond to different tissue structures or staining densities.

3D Intensity Map of Stain-Normalized Histopathology Image

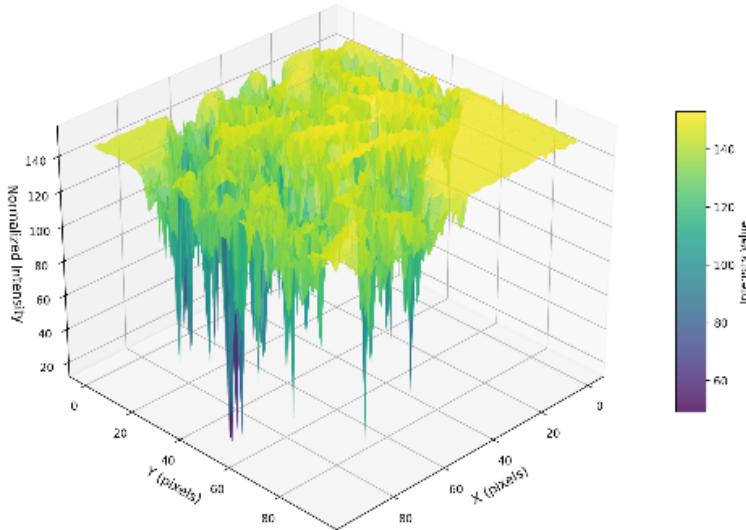


**Fig. 2.** 3D-Intensity Restructured Stainless Histopathology Image.

The transformation happened to the stain-normalized image into a grayscale intensity map, and it was visualized as a 3D surface plot. This plot provides a spatial representation of intensity variations across the tissue section, and highlight regions of high and low staining density. The peaks and valleys in the 3D plot correspond to areas of dense cellular material and less stained regions ( $I_{(norm)}(x, y)$ ), respectively. As shown in Table 1., the result indicated the 3D restructured stainless image has 0.83 to 0.93 SSIM indicating a minor loss from 2D to 3D conversion. By using the stain-normalized image for this transformation, the intensity values reflect true tissue characteristics rather than artifacts of staining variability.

## 5 Implications

### 5.1 Enhanced Diagnostic Accuracy and Consistency

Stain normalization serves as a crucial preprocessing strategy in computational pathology, and it functions as a domain adaptation technique that standardizes histopathology images from diverse sources [22]. This process addresses the real-world variability introduced by differences in staining protocols, reagent batches, and scanning equipment across hospitals and laboratories. By transforming images into a consistent color space, stain normalization ensures that both human pathologists and AI models receive uniform visual information [15]. Also, it enhances diagnostic consistency and enabling machine learning models to generalize effectively across datasets from different institutions [2, 12-14, 20]. The comparison between original and normalized images demonstrates significant improvements in image quality and analytical potential. The normalized image exhibits enhanced color standardization with

more uniform pink (eosin) and purple (hematoxylin) tones [23], effectively reducing the harsh color variations that characterized the original image. This standardization leads to improved contrast enhancement, and makes cellular structures more clearly delineated while creating greater background uniformity that eliminates potential confounding factors for automated analysis systems [3].

## 5.2 Theoretical Implication

The methodology's mathematical rigor is rooted in the application of the Beer-Lambert law, which models the absorption of light by tissue stains in a physically meaningful way [20]. By converting RGB values to optical density (vector) space, this approach captures the true interaction between light and stained tissue components and provides a more measurable and robust basis for normalization than simple color histogram matching [25]. This not only improves the reliability of downstream quantitative analyses but also ensures that the resulting images reflect genuine biological differences rather than technical artifacts, supporting more precise and reproducible cancer diagnoses.

## 6 Conclusion

This work represents a significant step (data preprocessing) toward fully automated cancer diagnosis systems. Based on the result, the 3D intensity stainless method remains rich feature representations for machine learning models and potentially enables the detection of subtle patterns. This research delivered several significant contributions to the field of computational pathology. First, it introduces a novel framework that moves beyond traditional 2D analysis by leveraging 3D intensity representations of tissue architecture. Second, the development of a mathematically rigorous stain normalization procedure based on the Beer-Lambert law provides a physically meaningful approach to standardizing histopathological images. Third, the integration of 3D CNN models with volumetric tissue information establishes a new paradigm for automated cancer detection systems.

There are a few limitations. First, the computational complexity and processing time requirements for 3D reconstruction and CNN classification warrant further investigation for practical clinical deployment. The method's robustness across diverse clinical settings, despite stain normalization improvements, requires broader validation studies to ensure reliable performance in real-world applications. In the future, the proposed method will be applied for cancer detection and classification CNN models in clinical settings.

## References

1. S. Mitra, B. Uma Shankar, *Inf. Sci.* 306, 111 (2015).
2. P. Huang et al., *Quant. Imaging Med. Surg.* 15, 636 (2025).
3. Md. Z. Hoque, A. Keskinarkaus, P. Nyberg, T. Seppänen, *Inf. Fusion* 102, 101997 (2024).
4. L. N. Sáenz, Doctoral dissertation, Universidad Carlos III de Madrid (2023).
5. T. A. A. Tosta et al., *Biomed. Signal Process. Control* 85, 104978 (2023).
6. H. Zhang et al., *Biophys. J.* 122, 4207 (2023).
7. P. Ruusuvuori et al., *Heliyon* 8, e08762 (2022).
8. T. A. A. Tosta et al., *Biomed. Signal Process. Control* 85, 104978 (2023).
9. K. Takahashi et al., *Tomography* 8, 131 (2022).

10. A. Naglah et al., *Sensors* 21, 3878 (2021).
11. J. T. C. Liu et al., *Nat. Biomed. Eng.* 5, 203 (2021).
12. X. Zheng et al., *Int. J. Intell. Syst.* 36, 6312 (2021).
13. L. Schneider et al., *Eur. J. Cancer* 160, 80 (2022).
14. R. S. Vanguri et al., *Nat. Cancer* 3, 1151 (2022).
15. K. N. Rao et al., *Proc. Int. Conf. Sustain. Comput. Smart Syst. (ICSCSS)*, 85 (2023).
16. P. Ruusuvuori et al., *Heliyon* 8, e08762 (2022).
17. B. Roy, M. Gupta, B. Krishna Goswami, *IEEE Access* 12, 93957 (2024).
18. P. Bankhead, *J. Pathol.* 257, 391 (2022).
19. A. A. Borkowski et al., *arXiv:1912.12142* (2019).
20. B. Zhao et al., *Comput. Electr. Eng.* 103, 108304 (2022).
21. V. Sureshkumar et al., *J. Pers. Med.* 14, 792 (2024).
22. M. Salvi, N. Michielli, F. Molinari, *Comput. Methods Programs Biomed.* 193, 105506 (2020).
23. M. Golberg et al., *Transl. Res. Anat.* 35, 100294 (2024).
24. P. Ruusuvuori et al., *Heliyon* 8, e08762 (2022).
25. A. Pulumati et al., *Cancer Rep.* 6, e1764 (2023).